Journal of Structural Geology 32 (2010) 1101–1113

Contents lists available at ScienceDirect

Journal of Structural Geology

journal homepage: www.elsevier.com/locate/jsg

Normal fault interactions, paleoearthquakes and growth in an active rift

A. Nicol [a,*], J.J. Walsh [b], P. Villamor [a], H. Seebeck [a], K.R. Berryman [a]

[a] GNS Science, PO Box 30368, Lower Hutt, New Zealand
[b] Fault Analysis Group, School of Geological Sciences, University College Dublin, Belfield, Dublin 4, Ireland

ARTICLE INFO

Article history:
Received 22 December 2009
Received in revised form
31 May 2010
Accepted 25 June 2010
Available online 24 July 2010

Keywords:
Fault interactions
Taupo rift
Paleoearthquakes
Kinematic coherence
Fault growth

ABSTRACT

Fault interactions are an essential feature of all fault systems on timescales of individual earthquakes to millions of years. We examine the role of these interactions in the development of an array of normal faults within the active Taupo Rift, New Zealand. Stratigraphic horizons (0–26 ka) exposed in 30 trenches and laterally extensive topographic surfaces (~18–340 ka) record displacements during surface-rupturing earthquakes over time intervals of up to 100's of thousands of years. Complementary changes in displacements, displacement rates and earthquake histories between faults are observed for along-strike displacement profiles and at points on fault traces. Variations of displacement are attributed mainly to fault interactions, and decrease with the aggregation of displacements on progressively more faults and over longer time intervals. Rift-wide displacement rates are, for example, near-constant over timescales of <60 kyr and suggest a level of order which is greater than that of individual fault traces. Each fault is, nevertheless, a vital element of a system that displays a remarkable degree of kinematic coherence which produces, and maintains, a hierarchy of fault size throughout the deformation history. As a consequence, on spatial scales greater than an individual fault trace and over temporal scales more than several earthquake cycles, the behaviour of individual faults can be relatively predictable. Fault interactions are accompanied by changes in fault system geometries consistent with increases in their maturity arising from strain localisation processes, including fault linkage and death.

1. Introduction

Fault interactions are an essential feature of fault systems (Walsh and Watterson, 1991). In circumstances where faults intersect (hard-linkage) or form relay ramps (soft-linkage) complementary displacement patterns on the component faults provide unequivocal kinematic evidence for their interaction (e.g., Peacock and Sanderson, 1991; Childs et al., 1995; Cartwright et al., 1995, 1996; Dawers and Anders, 1995; Nicol et al., 1996; Walsh et al., 2003a). As fault growth by increasing fault length and/or displacement is typically achieved via many increments of slip which accrue during earthquakes (Walsh and Watterson, 1987; Stein et al., 1988; Cowie and Scholz, 1992a; Nicol et al., 2005a), fault interactions require that both finite fault displacement and earthquake slip are complementary between faults (Fig. 1). Whether a fault system is hard-linked or soft-linked, fault interaction reflects the stress concentrations and shadows arising from short-term stress-dependent behaviour of earthquakes (e.g., Harris, 1998; Stein, 1999; King and Cocco, 2000; Robinson, 2004; Pondard et al., 2007). These stress studies together with analysis of paleoearthquakes on multiple faults within systems (e.g., Rockwell et al., 2000; Nicol et al., 2006; Dolan et al., 2007) suggest that faults may dynamically and kinematically interact over distances of tens of kilometres. These long-range interactions are, however, sometimes difficult to demonstrate kinematically because they produce displacement variations over the life span of the faults that are more subtle and less obviously complementary than is the case for well defined arrays of fault segments (compare faults 2 & 3 in Fig. 1).

Fault interactions have a profound impact on the dimensions and displacement accumulation of faults in systems over timescales of millions of years (Fig. 1). Many faults can, however, have near-constant lengths from an early stage in their history, with growth primarily achieved by increases in cumulative displacement rather than changes in fault length (Walsh et al., 2002; Childs et al., 2003; Schlagenhauf et al., 2008). Near-constant fault lengths are attributed to retardation of lateral propagation by interaction between fault tips. In systems where faults reach their final length early the maximum magnitude of subsequent earthquakes will also be constant. For faults of constant-length temporal variability in slip and recurrence of earthquakes may, in part, reflect migrations in the loci of strain accumulation associated with fault interactions (Wallace, 1987; Nicol et al., 2006). These interactions therefore

* Corresponding author. Fax: +64 4 570 4600
E-mail address: a.nicol@gns.cri.nz (A. Nicol).

0191-8141/$ – see front matter © 2010 Elsevier Ltd. All rights reserved.
doi:10.1016/j.jsg.2010.06.018

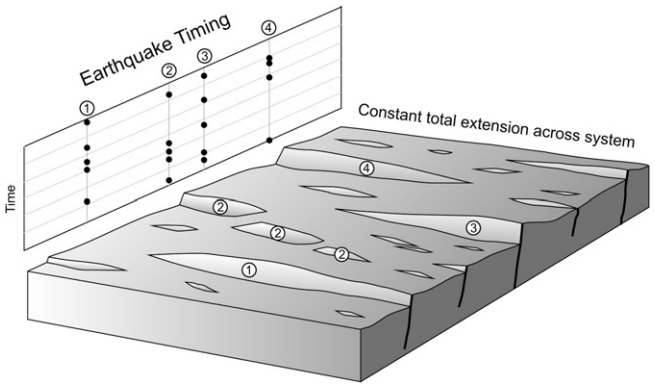

Fig. 1. Schematic block diagram showing displacements in a fault system and the role of interactions between faults in their development. Total extension is uniform for all transects across the system with changes in displacements on individual faults arising from interactions with nearby structures (see also Walsh and Watterson, 1991). Filled circles in the graph to the left of the block diagram indicate the timing of earthquakes on faults 1–4, which are the highest displacement structures in the array. Recurrence intervals of earthquakes on individual faults are variable and complementary; i.e. on timescales of at least the average recurrence interval of individual faults extension across the entire system is approximately uniform.

produce both variations in the earthquake process and, in circumstances where fault system boundary conditions are uniform, a hierarchy in which the longest faults move fastest, but with individual faults accruing displacement at near-constant rates over millions of years (Nicol et al., 1997, 2005b).

In this paper we examine the role of fault interactions on fault displacement accumulation over timescales ranging from individual earthquakes to 100's of thousands of years for a system of normal faults in the Taupo Rift, New Zealand (Fig. 2). This active rift, which is delineated by active fault traces and historical seismicity, generally forms a well defined graben 15–40 km wide (Fig. 2 cross-section) that started to form at about 1–2 Ma (Wilson et al., 1995) and comprises a dense array of active normal fault traces (Figs. 2, 3a and 4). The large number of active fault traces ($N > 300$) makes the Taupo Rift an excellent location to examine fault growth and the role of fault interaction. These interactions and associated fault growth are recorded using displacements of 0.2 m–550 m for time intervals of 1– ~340 kyr from offset topographic surfaces and near-surface stratigraphy in fault trenches (Fig. 3). Displacements provide information on the timing and slip of surface-rupturing earthquakes and on the accrual of displacement over time intervals up to 100's of thousands years.

The high density, short lengths and segmented nature of active fault traces are all hallmarks of a relatively immature fault system at the ground surface in the Taupo Rift (see Wesnousky, 1988; Cowie et al., 1993; Meyer et al., 2002; Schlagenhauf et al., 2008). This immaturity strongly impacts the fault displacement–length population and appears to decrease with depth (Seebeck, 2008), suggesting that the fault system has evolved through time. Our analysis also demonstrates that the accumulation of displacement of all faults in the system and the history of earthquakes that produce displacement increases are interdependent. Interactions between faults have a profound impact on their growth, a conclusion which we believe has wide application to other fault systems.

2. Fault system geology and data

Normal faults of the Taupo Rift accommodate near orthogonal extension of up to about 15 mm/yr in the central North Island of New Zealand (Villamor and Berryman, 2001; Wallace et al., 2004; Lamarche et al., 2006; Mouslopoulou et al., 2008; Begg and Mouslopoulou, 2010). The rift passes through two rhyolitic volcanic

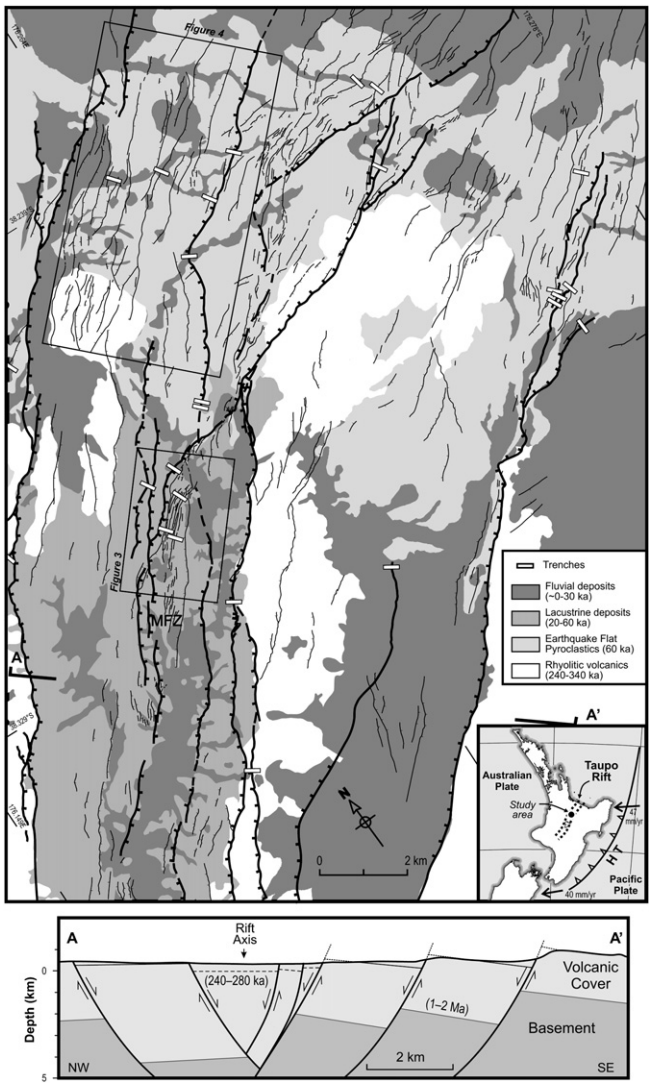

Fig. 2. Map of the Taupo Rift showing the locations of active faults and trenches (MFZ is the Maleme Fault Zone). Inset, North Island, New Zealand, plate boundary setting, with relative plate motion vectors from Beavan et al. (2002) and the location of the Hikurangi Trough (HT) shown. Cross-section A-A' across the entire rift shows the main faults and their displacements of the top Mesozoic basement (inferred from gravity data) and the top of 240–280 ka ignimbrites (see main map for section location).

centres outside the study area, however, this volcanism (including dike intrusion) does not appear to induce fault slip outside the volcanic centres where the faults are interpreted to be of tectonic origin (Seebeck and Nicol, 2009). Back-arc extension may have formed in response to clockwise rotation of the eastern North Island (relative to western North Island) associated with rollback of the subducting Pacific Plate, continental collision at the southern end of the Hikurangi margin and mantle buoyancy force (e.g., Walcott, 1987; Beanland and Haines, 1998; Wallace et al., 2004; Stratford and Stern, 2006; Nicol et al., 2007)(Fig. 2 inset). Normal faulting is thought to have initiated 1–2 Myr ago (Wilson et al., 1995) and produced a total crustal extension of ~20–60% on the syn-rift to basement boundary (Nicol et al., 2007; see also cross-section on Fig. 2).

This study focuses on a 15 km wide and 30 km long part of the rift comprising a dense array of active normal faults (e.g., Rowland and Sibson, 2001; Villamor and Berryman, 2001; Nairn, 2002; Acocella et al., 2003; Nicol et al., 2006; Seebeck, 2008; McClymont et al., 2009). The locations, lengths, and displacements of active normal faults exposed at the ground surface have been delineated using

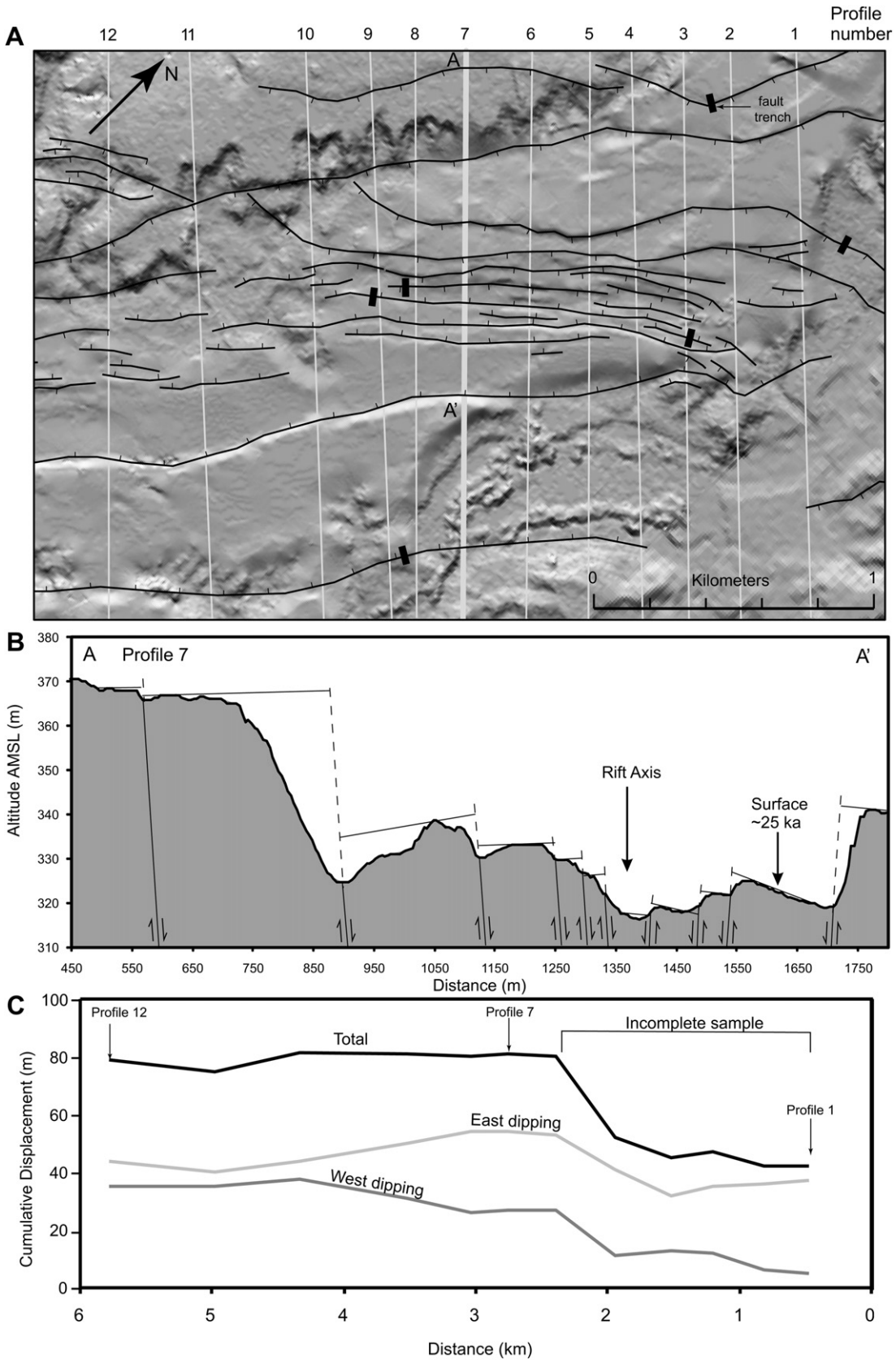

Fig. 3. (A) Fault map and DEM (illuminated from the NW) of the Maleme Fault zone at the rift axis. Ticks on faults indicate their dip and downthrow direction. (B) Topographic cross-section (profile 7 in A) illustrates the topographic expression of faults in the Taupo Rift where they displace a ~25 ka lacustrine/fluvial surface. (C) Cumulative displacement profiles for east dipping, west dipping and all faults constructed from 12 topographic profiles crossing the map area in (A). Variability of the total displacement chiefly arises because the sample is incomplete. Locations of trenches also shown in (A). See Fig. 2 for the map location.

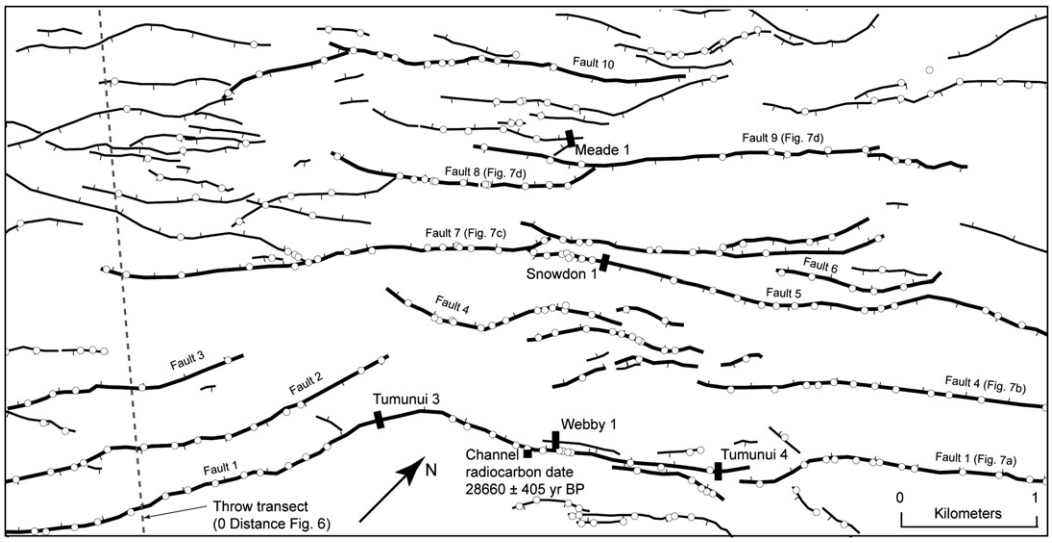

Fig. 4. Active fault map showing the locations of fault scarps up to ~40 m in height formed by displacement of the Earthquake Flat Surface (~60 ka) and abandoned stream channels. Locations of displacement measurements (open circles) and trench sites (black filled rectangles) are shown. Logs for the Meade 1, Snowdon 1 and Tumunui 3 trenches are shown in Fig. 5. Fault traces for displacement profiles presented in Fig. 6 are indicated by thick lines and by the fault numbers. See Fig. 2 for the map location.

a combination of ~1:17000 aerial photographs and digital elevation models (TOPSAR and GPS RTK surveying data) and tape and level. Although these data permit scarp heights of as little as 10–20 cm to be recorded, our dataset is probably incomplete for scarps < ~1–1.5 m high and 200 m long (Figs. 2, 3 and 4a). Active fault traces have average spacings of ~300–1000 m, strike northeast–southwest and dip steeply (~60–80° within 2 km of the ground surface), while fault scarps range in height, length and age up to 550 m, 28 km and ~340 ka, respectively (e.g., Villamor and Berryman, 2001; Nairn, 2002; Nicol et al., 2006; Berryman et al., 2008; Canora-Catalán et al., 2008; Seebeck and Nicol, 2009; McClymont et al., 2009). Fault intersections and segmentation are common in map view (Figs. 2–4). Where these segmented faults are <500 m apart across the rift and produce aggregated displacement profiles comparable to those of a single fault they are, for the purposes of this paper, considered to be a single structure. The high density, short lengths and segmented nature of active fault traces indicate that the fault system is immature at the ground surface (see also Walsh and Watterson, 1987, 1990; Walsh et al., 2003a). This immaturity is here attributed to the faults being rapidly buried by ignimbrite sheets and volcanic deposits (up to 1–2 km thick) formed in the past ~340 kyr and to the low cumulative extension recorded by the active fault traces since that time (≤~7% crustal extension, see cross-section in Fig. 2). The growth of normal faults in the rift may also, therefore, share similarities with, and have some implications for, the first few hundred thousand years of development of normal fault systems formed above reactivated faults (see Walsh et al., 2002).

Fault displacements (i.e. throws) have been recorded by vertical offsets of topographic surfaces (i.e. scarp heights). Key faulted volcanic, fluvial and lacustrine topographic surfaces range in age from ~18 to ~340 ka (e.g., Kennedy et al., 1978; Nairn, 1981, 2002; Villamor and Berryman, 2001). The most extensive of these surfaces is the top of the 60 ± 4 ka-old Earthquake Flat Pyroclastics (Nairn, 2002)(Fig. 2). Displacements on the ~60 ka surface have been recorded along the length of many faults. Additional throws on some of these faults were recorded by offsets of abandoned stream channels which mainly incised into the Earthquake Flat surface ~18–30 kyr ago. The ages of the incised channels is constrained by the age of the oldest deposits resting on fluvial gravels within the channels which range from ~18 ka to >~28 ka. For example, in Fig. 5a, b and c the estimated ages of the gravels are ~27, ~22 and ~18 ka respectively, while a calibrated radiocarbon date of 28660 ± 405 years BP (GNS Rafter Radiocarbon Laboratory, sample number *R* 29138/2) ~1.7 m above the Earthquake Flat Pyroclastics within an abandoned channel is consistent with its formation at ~30 ka (see Fig. 4 for channel and radiocarbon date location).

We use additional vertical displacements of stratigraphy exposed in 30 trenches excavated across 27 separate fault traces. The trench logs in Fig. 5 are examples from three fault traces each 1–2 km apart. The faults in each trench log displace a similar sequence of interbedded volcanic tephra and paleosols that range in age up to about 27, 22 and 18 ka in Fig. 5a, b and c, respectively. Displacement measurements from trenches include fault throw and near-fault bed rotations which have been discriminated from paleotopography using the geometry of gravel beds deposited subhorizontally. Trench stratigraphy record displacements on up to 11 volcanic air fall tephra layers (c. 10–40 cm average thicknesses) and multiple fluvial gravel deposits (e.g., Fig. 5). These volcanic layers, which were distinguished by their chemistry and mineralogy, and radiometrically dated fluvial deposits, range in age from ~1.7 ka to ~27 ka (e.g., Froggatt and Lowe, 1990; Nairn, 2002; Villamor and Berryman, 2001; Lowe et al., 2008). The available trench data permit displacement histories to be charted through time at four locations on fault 1 (see Fig. 4 for location) and at a single point on an additional 26 fault traces. These displacements together with those of topographic surfaces accumulated at rates of up to ~1.5 mm/yr on individual faults, with most of the faults having longer-term (>5 kyr) rates of <0.5 mm/yr (Villamor and Berryman, 2001; Nicol et al., 2006).

Trench data record displacements that accrued during earthquakes which ruptured the ground surface over the past 27 kyr. Fault scarps in the floors of abandoned river valleys, many of which have been trenched, suggest that most faults have experienced at least one surface-rupturing earthquake since the abandonment of fluvial surfaces ~18–30 kyr ago. These paleoearthquakes are inferred to range up to magnitude ~ Mw 6.8 (Villamor and Berryman, 2001), accommodate most of the extension in the rift and represent the greatest seismic hazard. Trenches reveal between three and eight surface-rupturing earthquakes on individual faults (e.g., Villamor and Berryman, 2001; Berryman et al., 2008; Canora-Catalán et al.,

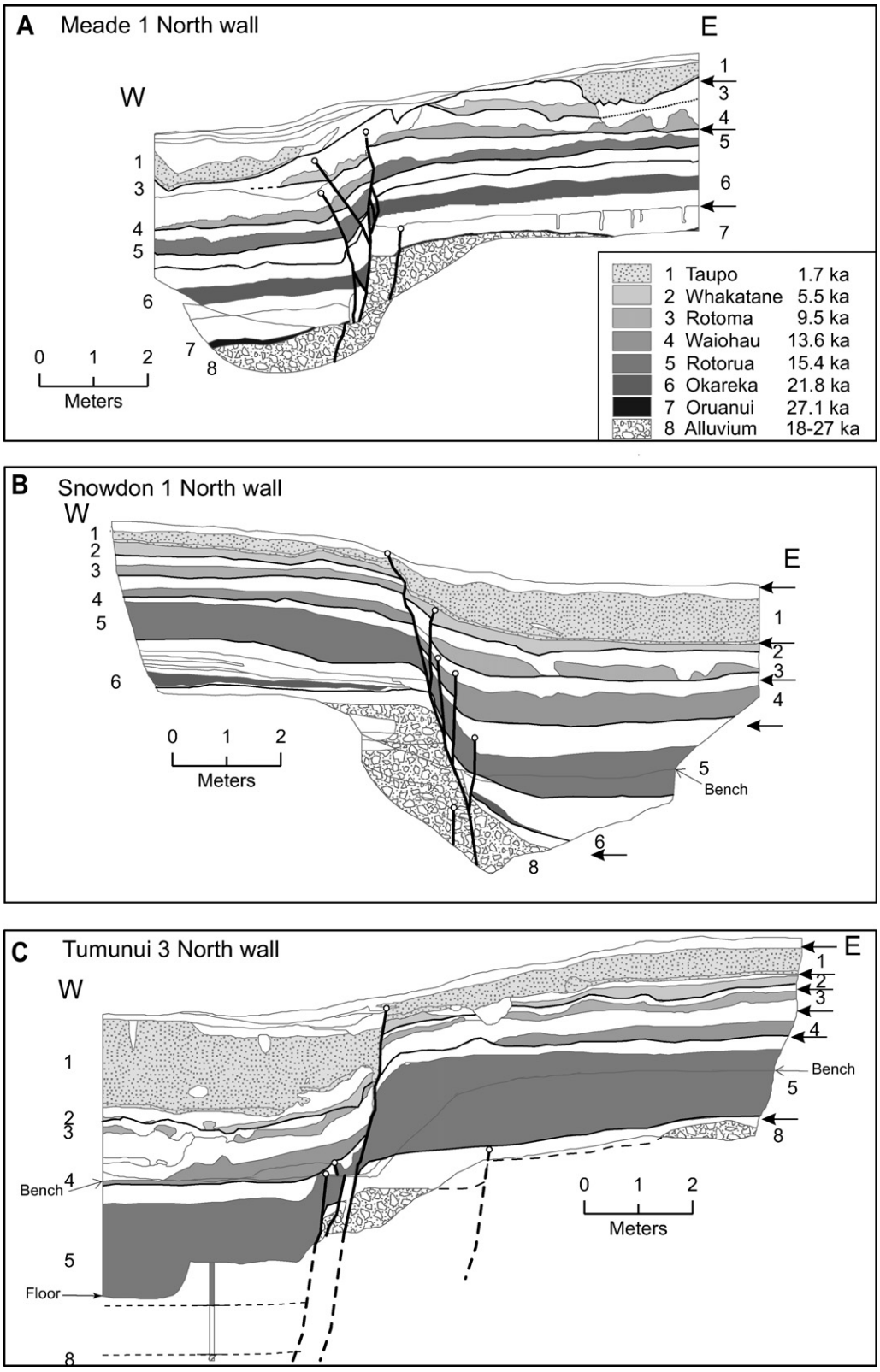

Fig. 5. Examples of trench logs for three fault traces within the Taupo Rift. The three logs, here referred to as Meade 1 (A), Snowdon 1 (B) and Tumunui 3 (C), sample similar stratigraphy (numbers on each log correspond to stratigraphy detailed in A), which is displaced by faults with displacements of up to ~2–3.3 m. Tephra (units 1–7) ages rounded to the nearest 0.1 ka are from Lowe et al. (2008). The estimated timing of paleoearthquakes is indicated by the horizontal filled arrows. The locations of the trenches are shown in Fig. 4.

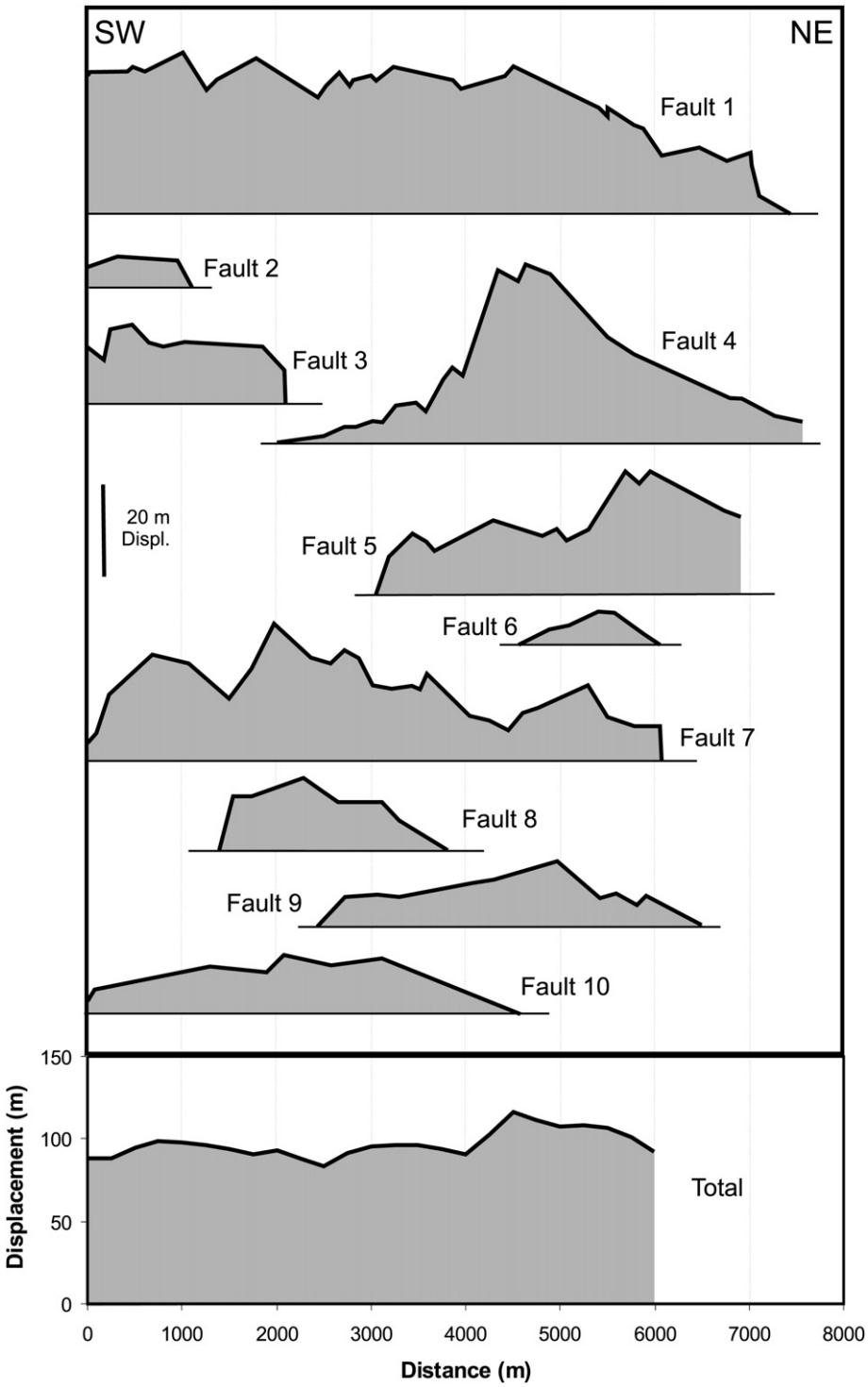

Fig. 6. Displacement profiles measured along strike on the ~60 ka Earthquake Flat topographic surface for faults 1–10 located in Fig. 4. Vertical scale is the same for all profiles (see 20 m displacement bar). Total displacement across the system of faults in the area of Fig. 4 has been summed along approximately northwest trending transects that are oriented approximately normal to the average fault strike and spaced at 250 m (the location of the zero distance transect is indicated on Fig. 4). Linear interpolation along faults is used to estimate displacements on transect lines where they do not coincide with displacement measurements. Sensitivity tests indicate that changing the trend of all transect lines by 10° or less does not significantly modify the total displacement profile.

2008; McClymont et al., 2009; this study). Logs from three of the trenches excavated are presented in Fig. 5 and have been used to determine the timing (e.g., see filled horizontal arrows on Fig. 5) and single-event displacement of prehistoric surface-rupturing earthquakes. Compilation of all earthquake data from the trenches indicate typical single-event displacements of 0.2–1.2 m and recurrence intervals of <1 to 14 kyr on individual fault traces (Nicol et al., 2009). These variations result in changes of displacement rates on many of the faults for timescales of <20 kyr, which have been attributed to fault interactions (Nicol et al., 2006, 2009).

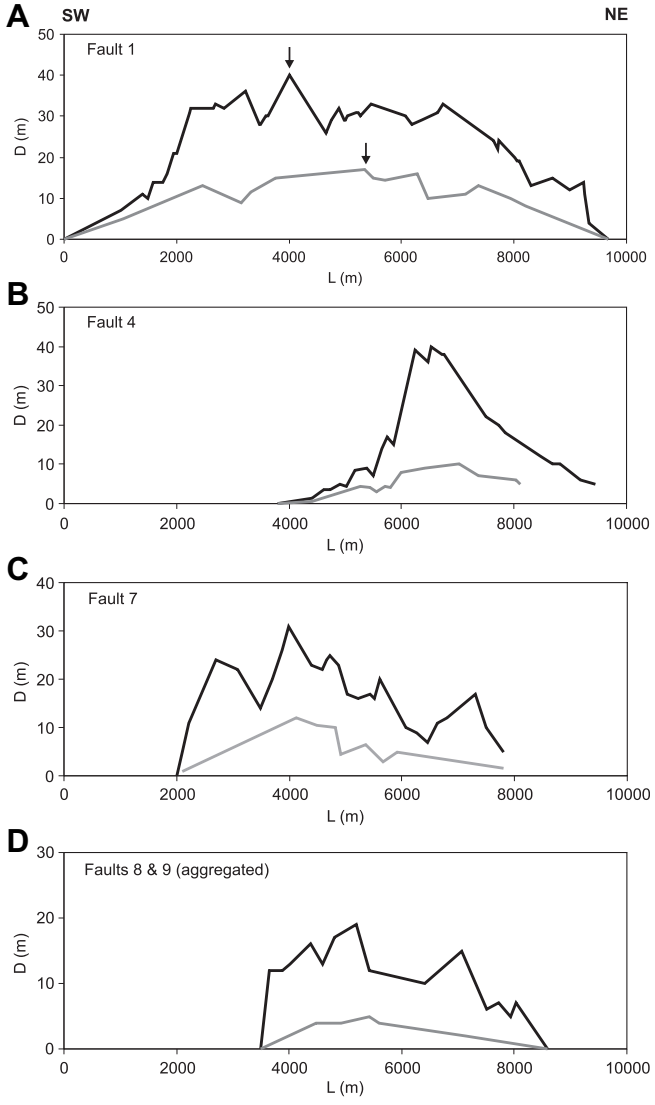

Fig. 7. Comparison of displacement profiles for the ~60 ka Earthquake Flat surface (black lines) and abandoned stream channels (~18–30 ka; grey lines) on faults 1 (A), 4 (B), 7 (C) and 8 & 9 (D). Profiles projected normal to fault strike onto a common plane striking at 040° with zero distance at the SW tip of fault 1. See Fig. 4 for fault locations.

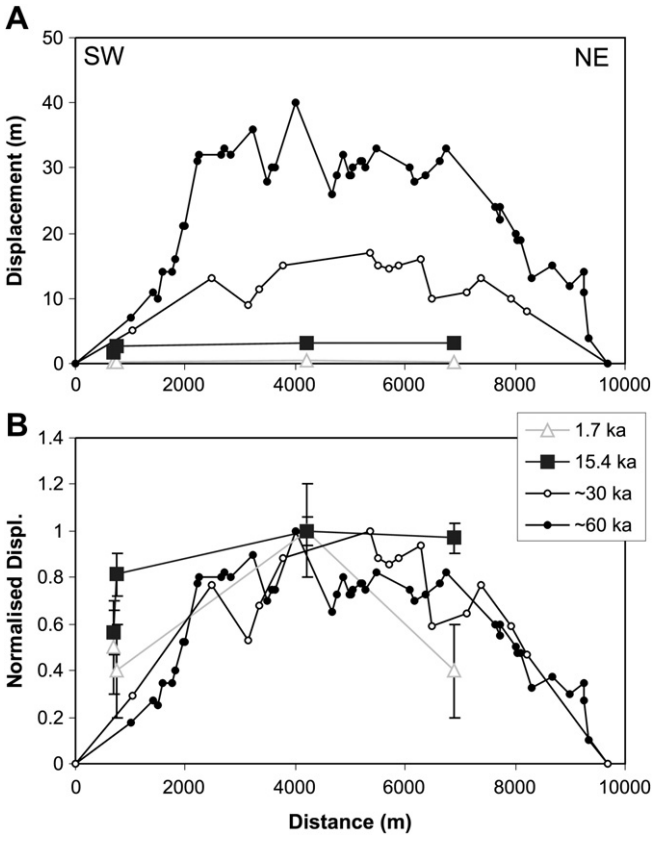

Fig. 8. Actual and normalised (to the maximum displacement) displacement profiles for the ~60, ~30, 15.4 and 1.7 ka horizons on fault 1. Displacements for the 15.4 and 1.7 ka horizons are from four trenches along the fault, which include Fig. 5C. See Fig. 4 for fault and trench locations.

3. Fault interactions

3.1. Strike-parallel displacement variations

Strike-parallel displacement profiles display variations in throw along the length of some of the faults on the Earthquake Flat surface and abandoned stream channels (Figs. 6–8). These displacement profiles show a range of geometries including approximately symmetrical bell-shaped (e.g., Fig. 7a), linear with an approximately centrally located maxima (Fig. 6 Fault 6), asymmetric with relatively steep gradients towards one tip (e.g., Fig. 6 Fault 8) and flat-topped profiles with high gradients at both tips (e.g., Fig. 6 Fault 7)(see also Muraoka and Kamata, 1983; Barnett et al., 1987; Walsh and Watterson, 1987, 1990; Peacock and Sanderson, 1991; Nicol et al., 1996; Manighetti et al., 2001; Schlagenhauf et al., 2008). Changes in the shapes of displacement profiles and associated variations in fault displacement gradients, appear to reflect the extent to which faults interact. For example, flat-topped or highly asymmetric profiles are associated with those faults that intersect, or relay displacement to adjacent faults (e.g., faults 2, 8 & 9, Figs. 6 and 7). By contrast the faults with the lowest displacement gradients tend to be those that are farthest from other faults of similar size (e.g., northern 2–3 km on fault 1, Fig. 7a). These observations are consistent with the view that lateral displacement gradients provide a measure of the degree of kinematic interaction between faults, with low displacement gradient faults interacting less than high gradient faults (e.g., Walsh and Watterson, 1990; Nicol et al., 1996).

All faults in the Taupo Rift are interacting, such that the sum of displacements across the rift (or part of the rift) is less variable than displacements on individual faults. This conclusion is consistent with the total displacements in Figs. 3c and 6 which represent the sum (perpendicular to fault average strike) of all throws on faults in two map areas that straddle the rift axis. The variability of displacement on the aggregate profiles (relative to the maximum displacement), which is partly due to incomplete sampling (see Fig. 3 caption for further discussion), is less than that of individual faults. The increase in stability of the system at higher cumulative displacements and greater spatial length scales suggests that, as with segmented faults (e.g., Childs et al., 1995), fault arrays in general are kinematically coherent systems in which the growth of each fault is related to all other faults in a given system (Walsh and Watterson, 1991).

Displacement profiles in Figs. 7 and 8 provide information about the lateral propagation of these faults. These profiles converge towards common points at, or close to, the tips of the mapped fault traces. Although we cannot discount some lateral propagation (e.g., because displacements of <1.5 m are sub-resolution and parts of

the fault close to its tip may not have been sampled), the approximately stable tip locations indicate that, within the resolution of the data, the faults in Fig. 7 have not propagated laterally over the past ~60 kyr. This conclusion is consistent with the view that many of the faults that now form active traces existed with their present strike-length prior to formation of the Earthquake Flat deposits. Following formation of the Earthquake Flat deposits, which may reach thicknesses of several hundred metres (Nairn, 2002), the faults propagated upwards during paleoearthquakes. The lack of evidence for lateral fault propagation also suggests that the observed changes in displacement profile shapes, which are similar to those reported in many other fault systems, are not due to variations in fault propagation rates (see Manighetti et al., 2001). By contrast, recent work has shown that a simple model of displacement accumulation on constant-length faults is capable of reproducing the main characteristics of the displacement profiles seen in Taupo and elsewhere, for a range of earthquake slip profiles and earthquake populations (Manzocchi et al., 2006).

To assess the temporal stability of displacement accumulation, profiles for the Earthquake Flat Surface and abandoned stream channels have been compared for four faults (Fig. 7). The general shapes of profiles Fig. 7c and d do not appear to change between the two sample intervals, with similar maximum displacement locations and asymmetries. By contrast, displacement profiles in Fig. 7a and b, which are for two faults with the same dip direction separated by about 1 km at the ground surface, appear to have changed between the two time intervals. In Fig. 7b the location of the maximum displacement remained approximately fixed, with displacement accumulation prior to stream channel incision focused in the central portion of the fault (i.e. ~6000–7500 m distance) producing a highly peaked displacement profile on the older surface. Displacement post channel formation is more flat-topped than displacements on the older horizon and, even when the large uncertainties on the age of the abandoned channels is accounted for, the rates of displacement in the centre of the fault decreased after channel formation. The profiles in Fig. 7a also display a change in distribution of displacements along the fault over time with the older Earthquake Flat displacements being slightly more asymmetric than the younger values from abandoned stream channels. This asymmetry requires a northeastward shift from about 3000–4000 m to 5000–5500 m in the location of the maximum displacement (see arrows Fig. 7a) and in the highest incremental displacement rates. One possible explanation for this temporal shift is that the faults in Fig. 7a and b are interacting, with the highest displacements on the 60 ka horizon in Fig. 7a occurring southwest of the highest displacements for the same horizon on the fault in Fig. 7b at distances of 6000–7500. For the post channel profiles the northeastward shift in maximum displacement in Fig. 7a (and an increase of displacement rates on this fault at distances of ~5000–7000 m) may have resulted in a decrease in the maximum displacement rates on the fault in Fig. 7b. These adjustments in displacement profiles may signal subtle changes in the earthquake slip over time periods of 10s of thousands of years, the consequence of which are explored in the next section.

3.2. Temporal displacement variations and paleoearthquakes

Dip-parallel displacement profiles have been constructed from fault-trench data (Fig. 5) and provide information about the timing and single-event displacement of earthquakes that ruptured the ground surface in the Taupo Rift (e.g., Villamor and Berryman, 2001; Berryman et al., 2008; Canora-Catalán et al., 2008; McClymont et al., 2009). The spatial and temporal relations of prehistoric earthquakes between faults have been examined using faulted stratigraphy exposed in trenches. In particular, prehistoric earthquakes have been identified using thickness changes of layers across faults, displacement decreases upwards along faults and the stratigraphic position of fault tips (e.g., see Fig. 5 for stratigraphic locations of paleoearthquakes). As with most other paleoseismic trench studies our estimates of the timing and slip for each event carry some uncertainty. Although some events have been dated to within several hundred years, the majority of these data constrain events to within ~2 kyr time windows, while single-event displacement measurements are typically ±0.1–0.2 m. Events with small slip of <~0.2 m are generally best inferred from the stratigraphic positions of fault tips. These small slip events are more likely to be sub-resolution than larger slip events, particularly in cases where they have been overprinted by later events. Therefore, the estimates of recurrence and single-event displacement may only apply for earthquakes with average slip of >0.2 m (i.e. magnitudes of >~5.5) and recurrence intervals >1 kyr (i.e. our measurements are maximums). In addition, it is not possible to be certain whether slip on two separate faults over the same two thousand year time interval, occurred synchronously or in different events. For these reasons we focus on comparing the general features of the earthquake histories and the broad shapes of the displacement–time curves between faults.

Displacement rates, recurrence intervals and single-event displacements vary temporally on the faults trenched (Figs. 8–10). Increases in displacement rates, and associated changes in earthquake

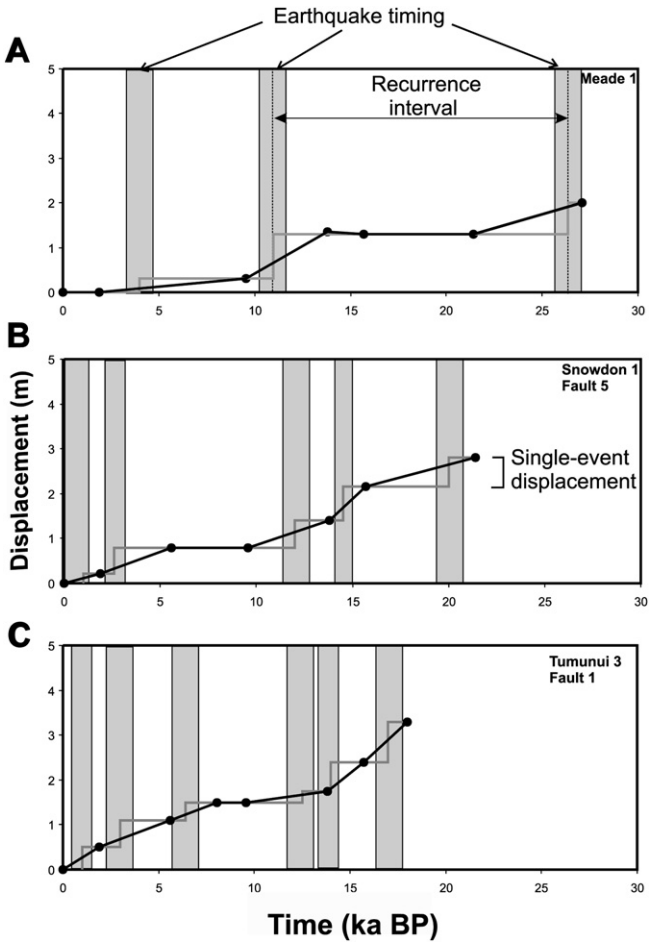

Fig. 9. Displacement–time plots for the faults exposed in the trenches presented in Fig. 5. Filled black circles indicate displacements of dated horizons, while the black line shows the displacement accumulation observed in each trench. The grey stepped line shows slip increments during individual paleoearthquakes. Inferred uncertainties in the timing of paleoearthquakes are indicted by the grey polygons.

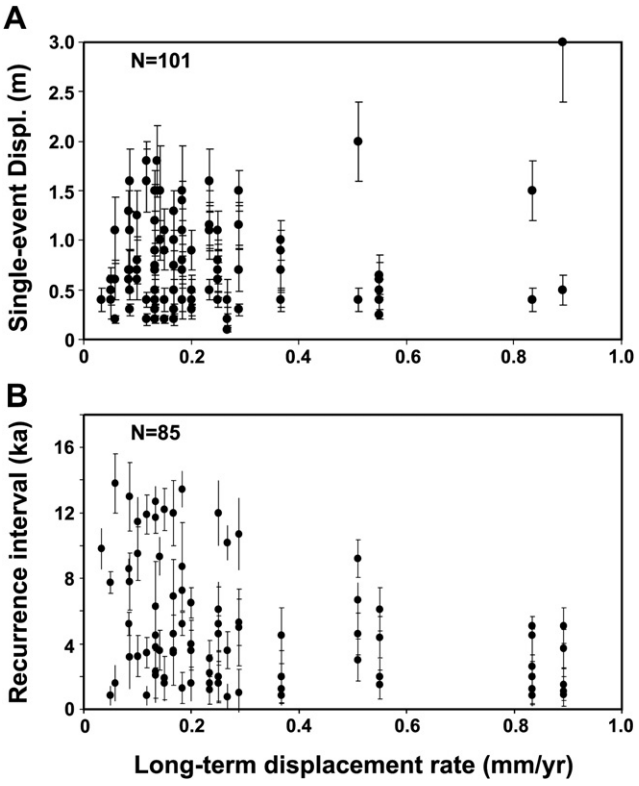

Fig. 10. Plot illustrating variations of earthquake single-event displacement and recurrence intervals for consecutive paleoearthquakes recorded in trenches across 26 individual fault traces in the Taupo Rift (e.g., Berryman et al., 2008). Single-event displacement and recurrence intervals of less than 0.1–0.2 m and 1–2 kyr, respectively, are sub-resolution and while their inclusion may modify the recurrence and slip populations, they are unlikely to entirely remove the variability of these earthquake parameters. Single-event displacement and recurrence intervals with a common long-term (~60 kyr) displacement rate indicate different earthquakes on the same fault.

recurrence intervals and single-event displacement, are not generally synchronous between fault traces, which suggests that triggered slip does not dominate the paleoearthquake data. Temporal changes in displacement rates (and earthquake slip and recurrence intervals) are supported by the displacement–time curves in Fig. 9 and are consistent with previous results (Nicol et al., 2006, 2009). Some variability in displacement rates and single-event displacement could arise because the trenches are point samples on traces along which finite and incremental displacements vary (Biasi and Weldon, 2006; Wesnousky, 2008). Trenching of fault 1 at four locations indicates that single-event displacement varies by up to a factor of three along the fault trace during individual earthquakes (e.g., throws on the 1.7 ka surface range from 0.2 to 0.5 m; Fig. 8a). In addition, it is possible that changes in slip distribution along fault traces also occur between earthquakes. Fig. 8b may suggest, for example, that the ~15 ka displacement profile is more flat-topped than the younger and older profiles (1.7, ~30 and ~60 ka) from which it could be inferred that cumulative slip during the three earthquakes between 1.7 and 15.4 ka resulted in higher displacements (relative to the maximum) along the southwestern-most ~3000 m of the fault than slip events during other time intervals over the past 60 kyr. Such changes in slip profiles between successive events could produce variations in displacement rate and single-event displacement at a point on fault traces of up to about a factor of two (compare normalised displacement for 1.7 and 15.4 ka horizons at a distance of ~600 m in Fig. 8), but cannot account for all of the factor of five or more (i.e., <0.2 to >1) variations in single-event displacement in most trenches. Unlike the single-event displacement, the timing of earthquakes estimated from each of the four trenches along fault 1 is the same, suggesting that these events ruptured at least ~70% of the fault length and, as long as the quality of the trench data are approximately uniform, the recurrence intervals should not change for different point samples along the trace.

We believe that a significant component of the variations of single-event displacement and recurrence (e.g., Figs. 9 and 10) are due to interactions between faults across the width of the rift. Fault interactions on timescales of thousands of years can be inferred by comparing the displacement histories of individual fault traces. Like the aggregated displacement profile in Fig. 6, trench displacements summed across fault zones and the entire rift show significantly less variability than is observed on individual fault traces (Nicol et al., 2006). The rift-wide displacement profiles indicate near-constant rates and suggest a level of order which is greater than that of the individual fault traces and the fault zones. Stable boundary conditions for the rift are consistent with models in which extension is driven by constant rates of plate motion (e.g., Beanland and Haines, 1998) and indicate that over the past 60 kyr, fluctuations of displacement rates on individual faults do not result from regional changes in strain rates imposed on faults from outside the system (e.g., volcanic or climatic forcing of fault slip accumulation). Over time intervals of thousands of years or more displacement accumulates systematically across the rift, with each fault being a component of a kinematically coherent system (see Walsh and Watterson, 1991). The fault interaction model is supported by static stress modelling of natural fault systems, including the Taupo Rift, indicating that the earthquake histories of individual faults are influenced by earthquakes on nearby faults (e.g., Harris, 1998; King and Cocco, 2000; Robinson, 2004; Pondard et al., 2007; Robinson et al., 2009). Fault interactions are a key element of such systems and over geological timescales (e.g., 10s of thousands to millions of years) are achieved by a combination of fault intersection and strains in the rock volume between faults. In this manner an array of interacting faults can be considered a single fault zone comprising multiple slip surfaces, with slip during each earthquake mainly concentrated on a single surface.

Variations in recurrence interval indicated for the fault traces in Fig. 9 are supported by data from all trenches (Fig. 10). For lower displacement rate faults (e.g., <0.4 mm/yr) the presence of some long recurrence intervals (10–15 kyrs) gives the appearance of these events being temporally clustered (Fig. 10b), as has been suggested for many other faults globally (e.g., Sieh et al., 1989; Marco et al., 1996). The constant rift boundary conditions and apparent temporal clustering of earthquakes require that earthquake activity migrates between faults in the rift over time, a phenomenon postulated for the Basin and Range (Wallace, 1987). Where the regional extension rates are uniform, migration of earthquake activity is implicit in changes of displacement rates on individual faults. Order of magnitude changes in displacement rates on timescales of <300 kyr are present in many fault systems (e.g., Mouslopoulou et al., 2009) and support the notion that spatial migration of earthquakes on timescales of thousands of years may be a process of widespread importance. As variations in earthquake recurrence appear to be higher for lower slip rate faults (Fig. 10b), we suggest that spatial migration of earthquake activity may have greatest impact on smaller faults whose earthquake histories are to some extent controlled by larger faults in the system (Nicol et al., 2006, 2009; Mouslopoulou et al., 2009; Robinson et al., 2009).

4. Displacement–Length relations and fault growth

The relation between displacement and length provides important information about the scaling properties and growth of

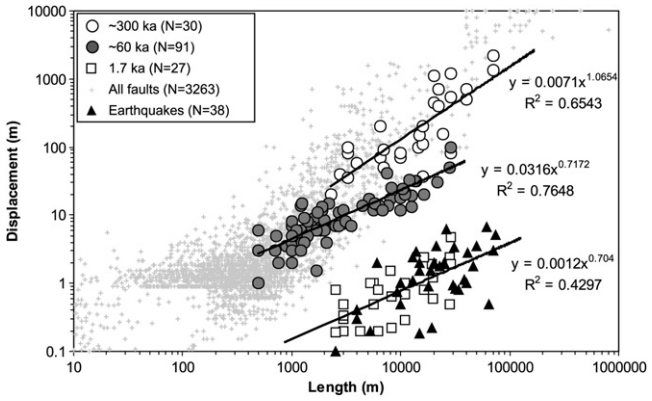

Fig. 11. Displacement–length plot for ~300 (open circles), 60 (grey filled circles) and 1.7 ka (open squares) horizons in the Taupo Rift together with global fault data (Bailey et al., 2005)(small grey crosses) and historical normal fault earthquakes (Stirling et al., 2002)(filled black triangles). Measurements for the ~300 ka horizon include data from the rift NE of the faulted region in Fig. 2 (Lamarche et al., 2006; Mouslopoulou et al., 2008). Lines of best fit for the Taupo Rift ~300, 60 and 1.7 ka horizons are least squares regressions on the *Y*-axis variable.

faults (Walsh and Watterson, 1988; Cowie and Scholz, 1992b; Gillespie et al., 1992; Schlische et al., 1996; Walsh et al., 2002; Bailey et al., 2005; Kim and Sanderson, 2005; Schultz et al., 2008). Displacement–length (D–L) plots for ancient fault systems typically reveal slopes of 1–1.5 over up to 8 orders of magnitude of displacement (e.g., Fig. 11 grey crosses), however, there remains debate about the precise slope of the power-law distribution. The positive D–L slope for ancient fault systems has been interpreted to represent a growth trend (e.g., Walsh and Watterson, 1988; Cowie and Scholz, 1992b). Alternatively, for those faults that do not grow significantly in length after relatively low amounts of basin extension (perhaps as low as 2–3%), near-vertical growth trends have been proposed (Walsh et al., 2002). The constant-length growth model of Walsh et al. (2002) has the advantage that it provides a rationale for the evolution of faults from individual earthquakes, which have lower displacements than ancient faults and an inferred D–L slope of about 1, to their final maximum displacements and lengths. The available displacement profiles in Fig. 7 provide support for the constant-length growth model in the Taupo Rift, at least for the past 60 kyr, and are consistent with the profile shapes predicted by Manzocchi et al. (2006) for a constant-length fault accommodating a range of earthquake populations with different earthquake slip profiles.

To examine the growth of faults in the Taupo Rift we have plotted displacement and length for ~300, 60 and 1.7 ka horizons along with global compilations for ancient faults (Bailey et al., 2005) and historical normal fault earthquakes (Stirling et al., 2002)(Fig. 11). Comparison of the global and Taupo D–L datasets suggests that the 1.7 ka Taupo measurements are similar to those of the global historical earthquakes. This similarity in D–L relations is compatible with the view that many of the 1.7 ka Taupo displacements accrued during single earthquakes, a conclusion which is consistent with estimates of the recurrence interval for the Taupo rift (Villamor and Berryman, 2001; Nicol et al., 2005b, 2009; Berryman et al., 2008; Canora-Catalán et al., 2008). Similarly, the ~300 ka Taupo Rift data plot within the field of the global data for ancient faults in Fig. 11 (compare open circles and grey crosses). As would be expected for a fault growth model involving displacement accumulation but with limited growth in fault length, such as the constant-length growth model of Walsh et al. (2002), the D–L data for the 60 ka horizon occupies a position which is intermediate between ancient faults and earthquakes. There is, however, one aspect of the D–L scaling, i.e. the slopes of D–L data distributions, which is not readily attributed to existing fault growth models and is briefly considered below.

Whilst D–L distribution for the ~300 ka Taupo horizon has a comparable slope to the ancient fault global dataset (i.e. 1–1.5), the lines of best fit for faults preserved in the 60 & 1.7 ka horizons have a slope of about 0.7. For the 1.7 ka faults the low slope is poorly defined by the widely spread data cloud ($R^2 = 0.4297$, see Fig. 11), and may not provide meaningful geological information about the growth of the fault system (other than to suggest that the D–L variations between earthquakes is greater than that for longer time intervals). The best fit D–L relationship for the 60 ka surface is, however, better defined than that of the younger horizon (i.e. $R^2 = 0.7648$, see Fig. 11) and therefore requires some explanation. Here we suggest that its low slope can be attributed to a combination of (i) sampling bias, (ii) fault system immaturity and (iii) fault interaction.

(i) Sampling bias: The bulk of our ~60 ka D–L data are from a TOPSAR digital elevation model of displaced geomorphic surfaces with a vertical resolution of ~1–1.5 m and which is subject to a number of sampling biases. These sampling biases arise because it is not possible to record faults, or parts of faults, that are below the resolution of the data (e.g., Watterson et al., 1996; Bailey et al., 2005). In our dataset displacements <~1.5 m are not always imaged in the topographic model resulting in an under-sampling of small faults (e.g., with throws <1.5 m), and a reduction in the measured lengths of some faults by at least 100–200 m; this is particularly important for those faults with lengths of <500 m. To reduce the impact of these sampling biases on Fig. 11 we have excluded faults with lengths of <500 m from the plot as our data may under-sample these fault lengths by a factor of 2 or more. We have also attempted to account for unmeasured fault lengths close to fault tips by using displacement gradients approaching the observed tips of mapped faults to estimate the actual tip location. Collectively these measures resulted in an increase in slope of the line of best fit by ~0.15 to the 0.7 observed in Fig. 11. Whilst there is every likelihood that this sampling bias also introduces a systematic under-sampling of low displacement faults longer than the 500 m threshold trace length, inevitably leading to a decrease in the observed slope of the D–L relation, cursory examination of the data distribution suggests that an unbiased slope of less than 1.0 is possible (Fig. 11).

(ii) Fault system im maturity: Another factor that may help to account for the low D–L slope of faults on the ~60 ka surface (Fig. 11) is the immaturity of the fault system, as indicated by the large number of relatively short (e.g., <4 km) interacting fault traces (Figs. 2–4). This immaturity is interpreted to be a near-surface (<2 km) phenomenon arising from upward propagation of normal faults into relatively unconsolidated volcanic deposits and ignimbrite sheets. The resulting spatially distributed faulting at the ground surface, which may in part reflect tip-line bifurcation and segmentation processes (e.g. Childs et al., 1995; Walsh et al., 2003a), is maintained because the extension recorded across the rift by active fault traces is low and no more than ~7% (i.e. significantly less than the ~20–60% crustal extension inferred to have accrued since ~1–2 Ma).

(iii) Fault interaction: The formation of highly segmented and complex fault arrays within an immature fault system will accentuate the importance of fault interactions and associated displacement transfer within the Taupo Rift, leading to local increases in displacement gradients close to fault tips. These

increases in displacement gradients result in an increase in the ratio of displacement to length which is likely to be particularly important for the many (>100) short (e.g., <4 km) interacting/intersecting faults that dominate the D–L data for the ~60 ka surface. Preferentially increasing the D–L ratio for shorter faults would have the effect of decreasing the slope of the displacement–lengths plots. If this effect is real, then the difference in slope and associated leftward convergence of the ~60 and 300 ka fault populations (Fig. 11) provides information about fault growth. Reconciling the ~60 ka displacements and lengths with those of the ~300 ka population could be achieved by; 1) preferential linkage of smaller faults or fault segments to form longer faults on which displacements continue to accrue (e.g., Cartwright et al., 1995; McLeod et al., 2000; Mansfield and Cartwright, 2001), and/or 2) preferential death or temporary abandonment of the smaller faults (e.g., <2 km)(e.g., Meyer et al., 2002). The preferential linkage of arrays of fault segments reflects the fact that these arrays most likely represent the uppermost parts of underlying single faults (Seebeck, 2008) and that smaller faults on D vs L plots actually represent soft-linked fault segments which inevitably have higher D:L ratios (Walsh et al., 2003a). The preferential death of smaller faults is an established feature of many fault systems and for those characterised by rapid fault propagation followed by prolonged displacement accumulation (i.e. the alternative fault growth model of Walsh et al., 2002), will inevitably lead to a progressive increase in D–L slope with fault growth. Both of these localisation processes will produce increases in fault system maturity between timescales of 60–300 kyr, resulting in an increase in slope of the finite fault displacement–length relations. If this fault system is analogous to faults forming above, and reactivating pre-existing faults, our observations suggest that in regions with strain rates of $\sim 5 \times 10^{-15}$ s^{-1} (such as the Taupo Rift) fault systems could increase significantly in maturity during their first 300 kyr of development.

5. Discussion and conclusions

In the Taupo Rift fault interactions are required to account for complementary changes in displacements, displacement rates and earthquake histories between faults. Variations of displacement are inferred to arise from fault interactions and decrease with aggregation of displacements for progressively more faults. Rift-wide displacement rates are near-constant over timescales of <60 kyr and suggest a level of order which is greater than that of the individual fault traces. Fault interactions over geological timescales are achieved by a combination of ductile deformations that accommodate displacement transfer (e.g. relay ramps in normal fault systems) and physical linkage of faults, with interaction reflecting the strain concentrations and shadows arising from short-term stress-dependent behaviour of faults. Each fault is an element of a system that displays a degree of kinematic coherence which produces, and maintains, a hierarchy of fault size throughout the deformation history. As a consequence, on spatial scales greater than an individual fault and over temporal scales greater than several earthquake cycles, the behaviour of individual faults can be relatively predictable. The fault interactions implicit in kinematically coherent systems discussed here are considered an essential feature of all fault systems and will have widespread application (see Walsh and Watterson, 1991). If, as we believe, fault interactions are ubiquitous in fault systems, then no faults can be considered completely isolated from all other faults. The concept of the ideal isolated fault (e.g., Watterson, 1986; Walsh and Watterson, 1988) does, however, remain a useful tool for identifying different degrees of interaction between faults and circumstances where other factors, including changes in the rheology of the faulted rock volume, have had an important impact on fault development.

Characterising the role of fault interactions is aided by the immaturity of the fault system in the Taupo Rift which contains many small (e.g., <4 km length) discontinuous traces (Fig. 2). Whether attributed to sampling bias (e.g. under-estimation of fault lengths) or to geological processes that produce relatively short high displacement faults, the low slope (0.7) of the D–L plot for the ~60 ka horizon (relative to the ~300 ka data) partly derives from the immaturity of the fault system. Increase in the slope of D–L relations with increasing duration of faulting is consistent with what would be expected from strain localisation processes. These processes result in strain accumulation being progressively focused on the larger faults in a system which grow (perhaps in part by segment linkage) at the expense, and in some cases result in the death, of smaller faults (e.g., Cowie et al., 1993, 2000; Meyer et al., 2002; Walsh et al., 2003b). In the extreme this localisation process results in strains for the entire system being focused onto a single active fault and may result in an increasing proportion of larger magnitude earthquakes in the system. Independent of the number of active faults in a system, kinematic coherence of these faults will require that their displacement aggregates as if they were part of a single structure.

Acknowledgements

This research was funded by the Marsden Fund and FRST in New Zealand, and by a UCD (Ireland) President's Fellowship. We thank Brent Alloway, John Begg, Carlos Costa, Ursula Cochran, Rob Langridge, Nicola Litchfield, Vasso Mouslopoulou, Mark Stirling, Kate Wilson and Adriaan Van Herk for assisting with the trenching and Ian Nairn for tephra identification. Ross Stein and Valerio Acocella are thanked for their constructive reviews.

References

Acocella, V., Spinks, K., Cole, J., Nicol, A., 2003. Oblique backarc rifting of Taupo volcanic zone, New Zealand. Tectonics 22 (4), 1045. doi:10.1029/2002TC001447.

Bailey, W.R., Walsh, J.J., Manzocchi, T., 2005. Fault populations, strain distribution and basement reactivation in the East Pennines Coalfield, U.K. Journal of Structural Geology 27, 913–928.

Barnett, J.A.M., Mortimer, J., Rippon, J.H., Walsh, J.J., Watterson, J., 1987. Displacement geometry in the volume containing a single normal fault. American Association of Petroleum Geologists Bulletin 71, 925–937.

Begg, J.G., Mouslopoulou, V., 2010. Analysis of late Holocene faulting within an active rift using lidar, Taupo Rift, New Zealand. Journal of Volcanology and Geothermal Research 190, 152–167. doi:10.1016/j.jvolgeores.2009.06.001.

Beavan, J., Tregoning, P., Bevis, B., Kato, T., Meertens, C., 2002. The motion and rigidity of the Pacific plate and implications for plate boundary deformation. Journal Geophysical Research 107 (B10), 2261. doi:10.1029/2001B000282.

Beanland, S., Haines, A.J., 1998. A kinematic model of active deformation in the North Island, New Zealand, determined from geological strain rates. New Zealand Journal of Geology and Geophysics 41, 311–323.

Berryman, K., Villamor, P., Nairn, I., Van Dissen, R., Begg, J., Lee, J., 2008. Late Quaternary surface rupture history of the Paeroa fault, Taupo rift, New Zealand. New Zealand Journal of Geology and Geophysics 51, 135–158.

Biasi, G.P., Weldon, R.J., 2006. Estimating surface rupture length and magnitude of Paleoearthquakes from point measurements of rupture displacement. Bulletin of the Seismological Society of America 96, 1612–1623. doi:10.1785/0120040172.

Canora-Catalán, C., Villamor, P., Berryman, K., Martínez-Diaz, J.J., Raen, T., 2008. Rupture history of the Whirinaki fault, an active normal fault in the Taupo rift, New Zealand. New Zealand Journal of Geology and Geophysics 51, 277–293.

Cartwright, J.A., Trudgill, B., Mansfield, C.S., 1995. Fault growth by segment linkage: an explanation for scatter in maximum displacement and trace length data from the Canyonlands Grabens of S.E. Utah. Journal of Structural Geology 17, 1319–1326.

Cartwright, J.A., Mansfield, C., Trudgill, B., 1996. The growth of normal faults by segment linkage. In: Buchanan, P.G., Nieuwland, D.A. (Eds.), Modern Developments in Structural Interpretation, Validation and Modelling. Geolology Society London, 99, pp. 163–177.

Childs, C., Watterson, J., Walsh, J.J., 1995. Fault overlap zones within developing normal fault systems. Journal of the Geological Society of London 152, 535–549.

Childs, C., Nicol, A., Walsh, J.J., Watterson, J., 2003. The growth and propagation of synsedimentary faults. Journal of Structural Geology 25, 633–648.
Cowie, P.A., Scholz, C.H., 1992a. Growth of faults by accumulation of seismic slip. Journal of Geophysical Research 97, 11085–11096.
Cowie, P.A., Scholz, C.H., 1992b. Physical explanation for the displacement–length relationship of faults using a post-yield fracture mechanics model. Journal of Structural Geology 14, 1133–1148.
Cowie, P.A., Vanneste, C., Sornette, D., 1993. Statistical physics model for the spatiotemporal evolution of faults. Journal of Geophysical Research 98 (B12), 21809–21821.
Cowie, P.A., Gupta, S., Dawers, N.H., 2000. Implications of fault array evolution for synrift depocentre development: insights from a numerical fault growth model. Basin Research 12, 241–261.
Dawers, N.H., Anders, M.H., 1995. Displacement–length scaling and fault linkage. Journal of Structural Geology 17, 607–614.
Dolan, J.F., Bowman, D.D., Sammis, C.G., 2007. Long-range and long-term fault interactions in Southern California. Geology 35, 855–858. doi:10.1130/G23789A.1.
Froggatt, P.C., Lowe, D.J., 1990. A review of Late Quaternary silicic and some other tephra formations from New Zealand; their stratigraphy, nomenclature, distribution, volume and age. New Zealand Journal of Geology and Geophysics 33, 89–109.
Gillespie, P.A., Walsh, J.J., Watterson, J., 1992. Limitations of dimension and displacement data from single faults and the consequences for data analysis and interpretation. Journal of Structural Geology 14, 1157–1172.
Harris, R., 1998. Introduction to special section: stress triggers, stress shadows, and implications for seismic hazard. Journal of Geophysical Research 103, 24347–24358.
Kennedy, N.M., Pullar, W.A., Pain, C.F., 1978. Late Quaternary landsurfaces and geomorphic changes in the Rotorua basin, North Island, New Zealand. New Zealand Journal of Science 21, 249–264.
Kim, Y., Sanderson, D., 2005. The relationship between displacement and length of faults. Earth-Science Reviews 68, 317–334.
King, G., Cocco, M., 2000. Fault interaction by elastic stress changes: new clues from earthquake sequences. Advances in Geophysics 44, 1–36.
Lamarche, G., Barnes, P.M., Bull, J.M., 2006. Faulting and extension rate over the last 20,000 years in the offshore Whakatane Graben, New Zealand continental shelf. Tectonics 25, TC4005. doi:10.1029/2005TC001886.
Lowe, D.J., Shane, P.A.R., Alloway, B.V.A., Newnham, R.M., 2008. Fingerprints and age models for widespread New Zealand tephra marker beds erupted since 30,000 years ago: a framework for NZ-INTIMATE. Quaternary Science Reviews 27 (2008), 95–126. doi:10.1016/j.quascirev.2007.01.013.
Manighetti, I., King, G.C.P., Gaudemer, Y., Scholz, C.H., Doubre, C., 2001. Slip accumulation and lateral propagation of active normal faults in Afar. Journal of Geophysical Research 106 (B7), 13667–13696.
Mansfield, C., Cartwright, J.A., 2001. Fault growth by linkage: observations and implications from analogue models. Journal of Structural Geology 23, 745–763.
Manzocchi, T., Walsh, J.J., Nicol, A., 2006. Displacement accumulation from earthquakes on isolated normal faults. Journal of Structural Geology 28, 1685–1693.
McClymont, A.F., Villamor, P., Green, A.G., 2009. Fault displacement accumulation and slip rate variability within the Taupo Rift (New Zealand) based on trench and 3-D ground penetrating radar data. Tectonics 28, TC4005. doi:10.1029/2008TC002334.
McLeod, A.E., Dawers, N.H., Underhill, J.R., 2000. The propagation and linkage of normal faults: insights from the Strathspey-Brent-Statfjord fault array, northern North Sea. Basin Research 12, 263–284.
Marco, S., Stein, M., Agnon, A., 1996. Long-term earthquake clustering: a 50,000-year paleoseismic record in the Dead Sea Graben. Journal of Geophysical Research 101 (B3), 6179–6191.
Meyer, V., Nicol, A., Childs, C., Walsh, J.J., Watterson, J., 2002. Progressive localisation of strain during the evolution of a normal fault system. Journal of Structural Geology 24, 1215–1231.
Mouslopoulou, V., Nicol, A., Walsh, J.J., Beetham, D., Stagpoole, V., 2008. Quaternary temporal stability of a regional strike-slip and rift fault intersection. Journal of Structural Geology 30 (4), 451–463.
Mouslopoulou, V., Walsh, J.J., Nicol, A., 2009. Fault displacement rates on a range of timescales. Earth and Planetary Science Letters 278, 186–197.
Muraoka, H., Kamata, H., 1983. Displacement distribution along minor fault traces. Journal of Structural Geology 5, 483–495.
Nairn, I.A., 1981. Some studies of the geology, volcanic history and geothermal resources of the Okataina Volcanic Centre, Taupo Volcanic Zone, New Zealand. Unpublished PhD thesis, Victoria University of Wellington, New Zealand.
Nairn, I.A., 2002. Geology of the Okataina Volcanic Centre, Scale 1:50 000. Institute of Geological & Nuclear Sciences Geological Map 25. 1 Sheet + 156 p. Institute of Geological & Nuclear Sciences Limited, Lower Hutt, New Zealand.
Nicol, A., Watterson, J., Walsh, J.J., Childs, C., 1996. The shapes, major axis orientations and displacement patterns of fault surfaces. Journal of Structural Geology 18 (2/3), 235–248.
Nicol, A., Walsh, J.J., Watterson, J., Underhill, J.R., 1997. Displacement rates of normal faults. Nature 390, 157–159.
Nicol, A., Walsh, J.J., Berryman, K., Nodder, S., 2005a. Growth of a normal fault by the accumulation of slip over millions of years. Journal of Structural Geology 27, 327–342.
Nicol, A., Walsh, J.J., Manzocchi, T., Morewood, N., 2005b. Displacement rates and average earthquake recurrence intervals on normal faults. Journal of Structural Geology 27, 541–551.
Nicol, A., Walsh, J., Berryman, K., Villamor, P., 2006. Interdependence of fault displacement rates and paleoearthquakes in an active rift. Geology 34 (10), 865–868. doi:10.1130/G22335.1.
Nicol, A., Mazengarb, C., Chanier, F., Rait, G., Uruski, C., Wallace, L., 2007. Tectonic evolution of the active Hikurangi subduction margin, New Zealand, since the Oligocene. Tectonics 26, TC4002. doi:10.1029/2006TC002090.
Nicol, A., Walsh, J., Mouslopoulou, V., Villamor, P., 2009. Earthquake histories and Holocene acceleration of fault displacement rates. Geology 37 (10), 911–914. doi:10.1130/G25765A.
Peacock, D.C.P., Sanderson, D.J., 1991. Displacements, segment linkage and relay ramps in normal fault zones. Journal of Structural Geology 13, 721–733.
Pondard, N., Armiji, R., King, G., Meyer, B., Flerit, F., 2007. Fault interactions in the Sea of Maramara pull-apart (North Anatolian Fault): earthquake clustering and propagating earthquake sequences. Geophysical Journal International 171, 1185–1197.
Robinson, R., 2004. Potential earthquake triggering in a complex fault network: the northern South Island, New Zealand. Geophysical Journal International 159, 734–748.
Robinson, R., Nicol, A., Walsh, J.J., Villamor, P., 2009. Features of earthquake occurrence in a complex normal fault network: results from a synthetic seismicity model of the Taupo Rift, New Zealand. Journal of Geophysical Research 114, B12306. doi:10.1029/2008JB006231.
Rockwell, T.K., Lindvall, S., Herzberg, M., Murbach, D., Dawson, T., Berger, G., 2000. Paleoseismology of the Johnson Valley, Kickapoo, and Homestead Valley faults: clustering of earthquakes in the eastern California shear zone. Bulletin of the Seismological Society of America 90, 1200–1236.
Rowland, J.V., Sibson, R.H., 2001. Extensional fault kinematics within the Taupo volcanic zone, New Zealand, soft-linked segmentation of a continental rift system. New Zealand Journal of Geology and Geophysics 44, 271–283.
Schlische, R.W., Young, S.S., Ackermann, R.V., Gupta, A., 1996. Geometry and scaling relations of a population of very small rift-related normal faults. Geology 24, 683–686.
Schlagenhauf, A., Manighetti, I., Malavieille, J., Dominguez, S., 2008. Incremental growth of normal faults: insights from a laser-equipped analog experiment. Earth and Planetary Science Letters 273, 299–311.
Schultz, R.A., Soliva, R., Fossen, H., Okubo, C.H., Reeves, D.M., 2008. Dependence of displacement–length scaling relations for fractures and deformation bands on the volumetric changes across them. Journal of Structural Geology 30, 1405–1411.
Seebeck, H., Nicol, A., 2009. Dike intrusion and displacement accumulation at the intersection of the Okataina volcanic centre and Paeroa fault zone, New Zealand. Tectonophysics 475 (3–4), 575–685. doi:10.1016/j.tecto.2009.07.009.
Seebeck, H., 2008. The interrelationships between faulting and volcanism in the Okataina volcanic centre, New Zealand. Unpublished MSc Thesis, Victoria University of Wellington, Wellington.
Sieh, K.E., Stuiver, M., Brillinger, D., 1989. A more precise chronology of earthquakes produced by the San Andreas Fault in southern California. Journal of Geophysical Research 94, 603–623.
Stratford, W.R., Stern, T.A., 2006. Crust and upper mantle structure of a continental backarc: central North Island, New Zealand. Geophysics Journal International. doi:10.1111/j.1365–246X.2006.02967.x.
Stein, R., 1999. The Role of stress transfer in earthquake occurrence. Nature 402, 605–609.
Stein, R.S., King, G.C., Rundle, J.B., 1988. The growth of geological structures by repeated earthquakes. 2 Field examples of continental dip-slip faults. Journal of Geophysical Research 93, 13319–13331.
Stirling, M.W., Rhoades, D.A., Berryman, K.R., 2002. Comparison of earthquake scaling relations derived from data of the instrumental and pre-instrumental era. Bulletin of the Seismological Society of America 92, 812–830.
Villamor, P., Berryman, K., 2001. A late Quaternary extension rate in the Taupo volcanic zone, New Zealand, derived from fault slip data. New Zealand Journal of Geology and Geophysics 44, 243–269.
Walcott, R.I., 1987. Geodetic strain and the deformation history of the North Island of New Zealand during the late Cainozoic. Philosophical Transactions of the Royal Society of London 321, 163–181.
Wallace, L.M., Beavan, J., McCaffrey, R., Darby, D., 2004. Subduction zone coupling and tectonic block rotations in the North Island, New Zealand. Journal of Geophysical Research 109, B12406.
Wallace, R.E., 1987. Grouping and migration of surface faulting and variations in slip rates on faults in the Great Basin Province. Bulletin of the Seismological Society of America 77, 868–876.
Walsh, J.J., Watterson, J., 1987. Distributions of cumulative displacement and seismic slip on a single normal fault surface. Journal of Structural Geology 9 (8), 1039–1046.
Walsh, J.J., Watterson, J., 1988. Analysis of the relationship between displacements and dimensions of faults. Journal of Structural Geology 10, 239–247.
Walsh, J.J., Watterson, J., 1990. New methods of fault projection for coalmine planning. Proceedings of the Yorkshire Geological Society 48, 209–219.
Walsh, J.J., Watterson, J., 1991. Geometric and kinematic coherence and scale effects in normal fault systems. In: Roberts, A.M., Yielding, G., Freeman, B. (Eds.), The Geometry of Normal Faults. Geological Society Special Publication, 56, pp. 193–203.

Walsh, J.J., Nicol, A., Childs, C., 2002. An alternative model for the growth of faults. Journal of Structural Geology 24, 1669–1675.
Walsh, J.J., Bailey, W.R., Childs, C., Nicol, A., Bonson, C.G., 2003a. Formation of segmented normal faults: a 3-D perspective. Journal of Structural Geology 25, 1251–1262.
Walsh, J.J., Childs, C., Imber, J., Manzocchi, T., Watterson, J., Nell, P.A.R., 2003b. Strain localisation and population changes during fault system growth within the inner Moray Firth, northern North Sea. Journal of Structural Geology 25, 1897–1911.
Watterson, J., 1986. Fault dimensions, displacements and growth. Pure and Applied Geophysics 124, 365–373.
Watterson, J., Walsh, J.J., Gillespie, P.A., Easton, S., 1996. Scaling systematics of fault sizes on a large scale range fault map. Journal of Structural Geology 18, 199–214.
Wesnousky, S.G., 1988. Seismological and structural evolution of strike slip faults. Nature 335, 340–343.
Wesnousky, S.G., 2008. Displacement and geometrical characteristics of earthquake surface ruptures: issues and implications for seismic-hazard analysis and the process of earthquake rupture. Bulletin of the Seismological Society of America 98, 1609–1632. doi:10.1785/0120070111.
Wilson, C.J.N., Houghton, B.F., McWilliams, M.O., Lanphere, M.A., Weaver, S.D., Briggs, R.M., 1995. Volcanic and structural evolution of Taupo volcanic zone, New Zealand, a review. Journal of Volcanology and Geothermal Research 68, 1–28.